LA-UR-79-2329

TITLE: THE USE OF LASERS FOR ACCELERATOR DIAGNOSTICS: I. ELEMENTARY CONCEPTS

AUTHOR(S): J. P. Aldridge
T. D. Hayward

SUBMITTED TO: 8th Symposium On Engineering Problems of FusionResearch
San Francisco, California, NOVEMBER 13-16,1979

University of California

LOS ALAMOS SCIENTIFIC LABORATORY
Post Office Box 1663 Los Alamos, New Mexico 87545
An Affirmative Action/Equal Opportunity Employer

Form No. 836 R3
St. No. 2629
12/78

UNITED STATES
DEPARTMENT OF ENERGY
CONTRACT W-7405-ENG. 36

THE USE OF LASERS FOR ACCELERATOR DIAGNOSTICS: I. ELEMENTARY CONCEPTS

J. P. Aldridge and T. D. Hayward
Los Alamos Scientific Laboratory
Los Alamos, NM 87545

INTRODUCTION

The coming development of high current linear accelerators for H^- ions requires improvement in diagnostic instrumentation that will permit accurate determination of the occupied phase space. We propose to use a laser photodetachment method to provide this new capability.

The use of a laser for measuring emittance growth in particle accelerators is based on producing a neutral species from the particle being accelerated. In this way the influence of the accelerator's electric and magnetic fields and the space charge effects of the remaining beam on the particle trajectory ceases at the point of production. Thus, it is possible to probe the beam configuration at points normally inaccessible to diagnostic instruments such as in the acceleration gap of a linac or within a drift tube. The only perturbation introduced by the use of such a diagnostic is that produced by the small hole required to introduce the light into the cavity.

In this paper, we explore the fundamental processes that are operative and consider limitations to the accuracy of measurements using this diagnostic. Questions to be addressed subsequently include the experimental arrangement required to reconstruct the detailed beam profile from the measurements at several angles.

BASIC PROCESSES FOR H⁻ DIAGNOSTICS

The Nd:YAG laser produces a photon of energy 1.16 eV (λ = 1.064 μm) that is sufficient to remove the extra electron from H^-. The H^- binding energy is 0.75 eV.[1] This laser can be mode-locked to produce pulses as short as 25 ps. (A more normal configuration is a pulsed [Q-switched] laser that has a 20 ns pulse that can be controlled with approximately nanosecond jitter.) The mode locking process is carried out with a mode locking dye in the laser cavity so that there is no control over the time the train of pulses begins. This means that the light pulse itself must be used as a trigger for subsequent events. Among such events are switching a single pulse out of the train, triggering fast detection electronics such as a streak camera, and establishing the relationship of the light pulse with respect to the linac beam micropulse. The laser we are using is a commercial laser made by Quantel International and will produce pulses at 10 pulses per second with pulse energies up to 30 mJ per pulse.

The cross section (σ) for photodetachment as a function of wavelength is illustrated in Fig. 1 (Ref. 2). The Nd:YAG wavelength corresponds to the lower side of the peak. The cross section value is about 4×10^{-17} cm^2. The fraction, f, of H^- atoms photodetached in a single laser pulse is related to the laser fluence (in photons/cm^2/pulse) Φ, by

$$f = 1 - \exp(-\sigma\Phi) \qquad (1)$$

The assumption involved in deriving this equation, that the laser intensity does not change appreciably, is well satisfied for this case. A convenient

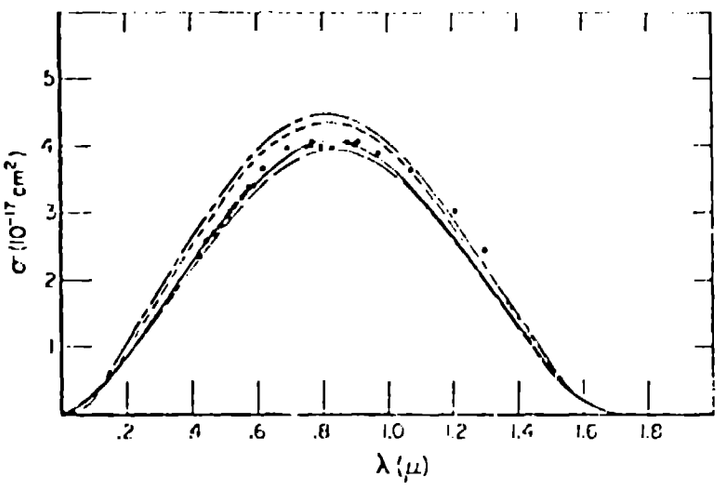

FIG. 1. The experimental photodetachment cross section for H⁻ (black dots) is compared with four theoretical calculations. All of these calculations used dipole velocity matrix elements with the Hart-Herzberg 20-parameter bound state wave function. The continuum functions used were: (— · — · —), static central field (Chandrasekhar and Elbert, 1.58); (- - -), plane wave (Chandrasekhar, 1948); (· · ·) exchange central field (John, 1960); (— · —) variational (Geltman and Krauss, 1960). Here the experimental points are normalized to the exchange central field calculation at 5280 Å.

characterization is the laser fluence required to remove half the particles. This is given by

$$\Phi_{1/2} = \ell n 2/\sigma \qquad (2)$$

or 1.73×10^{16} photons per pulse per cm^2. Using the formula that the photon energy E(eV) = 1.2395/λ (μm), this translates to an energy fluence of 3.23 mJ/cm^2/pulse. Thus the laser is, in principle, capable of removing all of the H^- ions in a 1 cm^2 area, a size sufficient for most accelerator gaps. However, we also would like to spatially define the particle beam by focusing the laser to a 100 μm (0.1 mm) diameter. (This is possible with a 30 cm focal length lens, a convenient distance from the accelerator axis.) The beam area is then reduced to 8×10^{-5} cm^2 with the consequence that the pulse energy needs only 0.25 μJ per pulse for 50% detachment. This dramatic overkill factor permits considerable experimental flexibility by reflection. We will elaborate below.

Since there is excess energy in the detachment process in spectral regions where the cross section is large, the recoil momentum of the hydrogen atom will introduce an angular spread in the detected particle distribution. Because the direction of the photodetached electron in the cm system is random, this represents a spread in the momentum distribution that is a lower limit to the H^- spread that can be detected. Figure 2 shows a velocity diagram for the photodetachment process.

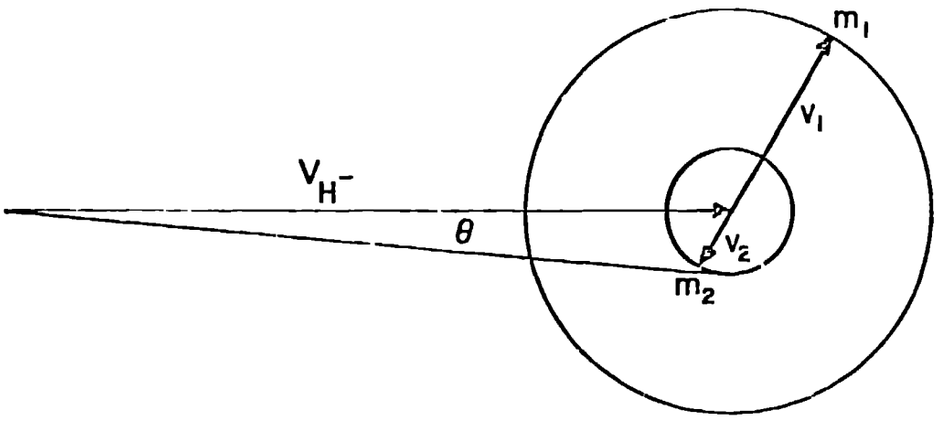

Fig. 2. Velocity diagram for photodetachment or photodissociation: m_1 represents the light particle and m_2 represents the heavy particle.

The photon momentum is totally negligible. This leads to

$$m_1 v_1 = m_2 v_2 \tag{3}$$

and

$$\frac{1}{2} m_1 v_1^2 + \frac{1}{2} m_2 v_2^2 = E_{photon} - E_{diss} = \Delta E \tag{4}$$

Thus the maximum transverse momentum of the H atom is

$$P_t = m_2 v_2 = \left[\frac{2m_2 \Delta E}{1 + m_2/m_1} \right]^{1/2} \tag{5}$$

and an angular spread is

$$\theta = \sin^{-1} \left[\frac{m_1}{m_2} \frac{\Delta E}{E} \right]^{1/2}$$

For H^-, particle 1 is an electron and particle 2 is the H atom. Thus

$$\theta \approx 14.8 \text{ μradians} / \sqrt{E(\text{MeV})} \tag{6}$$

This curve is plotted as Fig. 3. Although this result does not include relativistic effects, there should be only minor differences when these are included. For the measurements near the input of our test stand linac (E = 0.250 MeV) the lower limit of angular divergence we can expect to measure is about 30 μradians.

The fundamental physics of the diagnostic is extremely simple and means that attention to development work can be directed toward areas of detection and interpretation. These problems are very similar to those encountered with other more conventional forms of diagnostic apparatus such as wire scanners or harps.

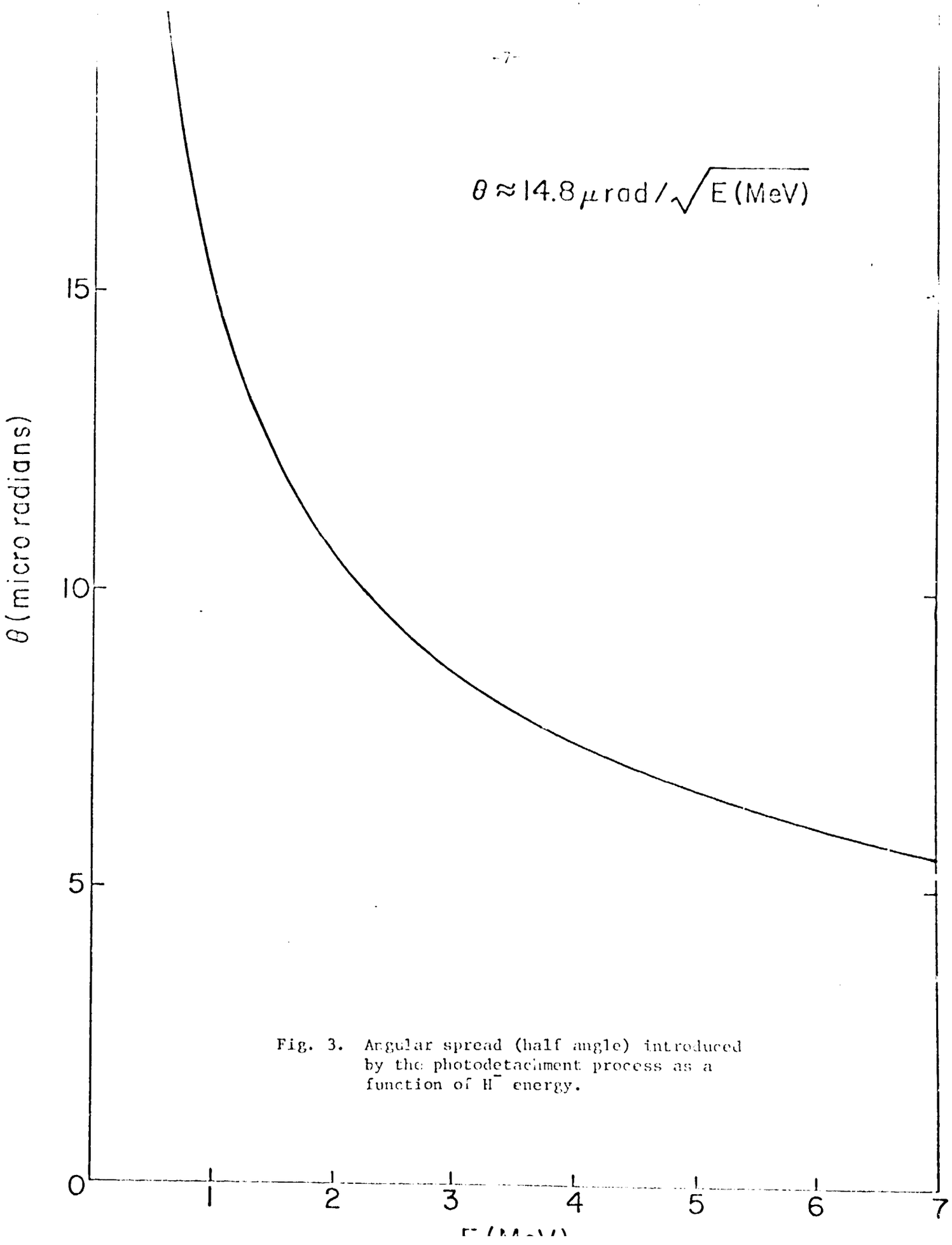

Fig. 3. Angular spread (half angle) introduced by the photodetachment process as a function of H^- energy.

TABLE I

APPROXIMATE DISSOCIATION ENERGIES FOR $H_2^+ \rightarrow H + H^+$

(From Ref. 3 for $1s\sigma_g - 2p\sigma_u$ Transition)

Level	Approximate Vertical* Dissociation Energy(eV)	o λ(A)	ΔE** (eV)	Relative Intensity From Arc Source
ground state (v = 0)	10.54	1175	7.89	0.38
v = 1	8.62	1440	5.97	0.83
v = 2	7.20	1720	4.55	1.00
v = 3	5.34	2320	2.69	0.90
v = 4	4.32	2870	1.67	0.71
v = 5	3.15	3935	0.50	0.46

* These values were read from Fig. 4 and thus must be regarded as approximate. The absorption spectra will be broad so that the energy given will be near the center of a wide distribution.

** Ground state dissociation energy = 2.6481 eV (Ref. 5).

An interesting aside is that it is possible to use the laser to detect H_2^+ surrogates for D^+. The energy diagram is shown in Fig. 4. Due to the Franck-Condon principle that the optical transition must be vertical, the energy required to photodissociate the H_2^+ is about 11.6 eV, well beyond conveniently available technology for high powered lasers (10.5 eV laser photons have been produced by Harris, et al[4] by frequency tripling in metal vapors). However, for vibrationally excited H_2^+, the energy required drops rapidly with vibrational quantum number. The distribution over vibrational states for H_2^+ produced in an arc is also included in Fig. 4 (see also Table I). There appears then to be enough population in the excited states to be photodissociated by a visible or near uv laser.

Since the two fragments are now nearly equal in mass, the excess energy is nearly equally divided and the spread becomes $0 \approx [\Delta E/E]^{1/2}$. This relation for various excited levels is presented in Fig. 5.

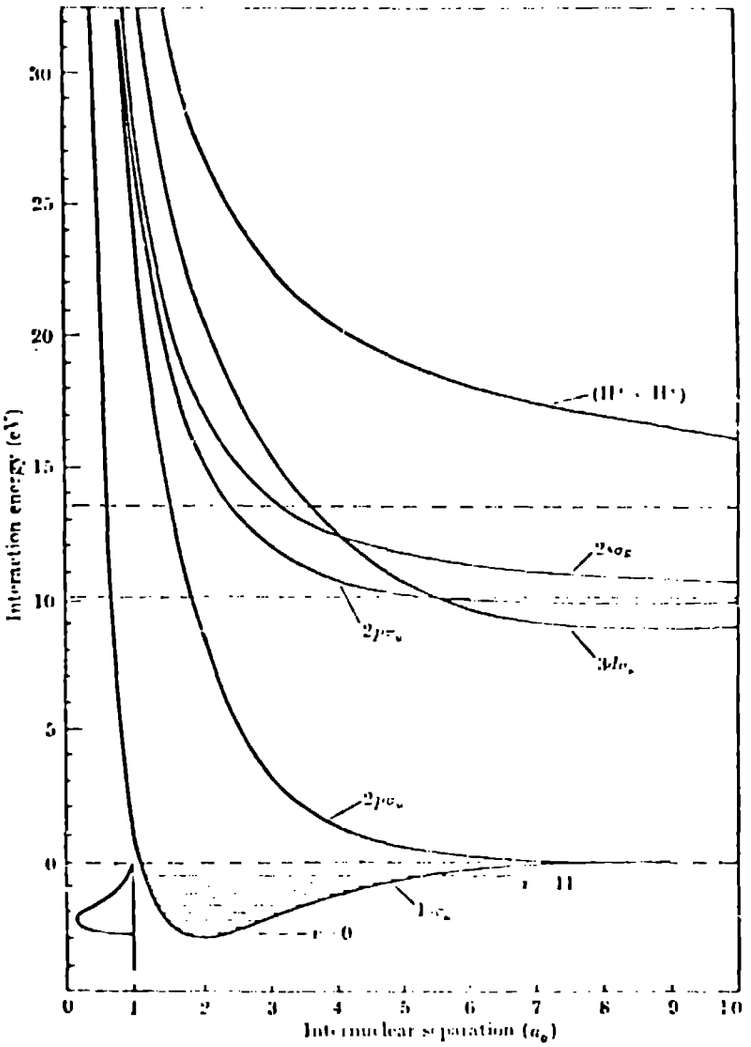

FIG. 4. Potential energy curves for various states of H_2^+. The vibrational levels associated with the ground electronic state are shown together with the relative probability of population of the different levels when the H_2^+ is produced by electron impact excitation from the ground state of H_2.

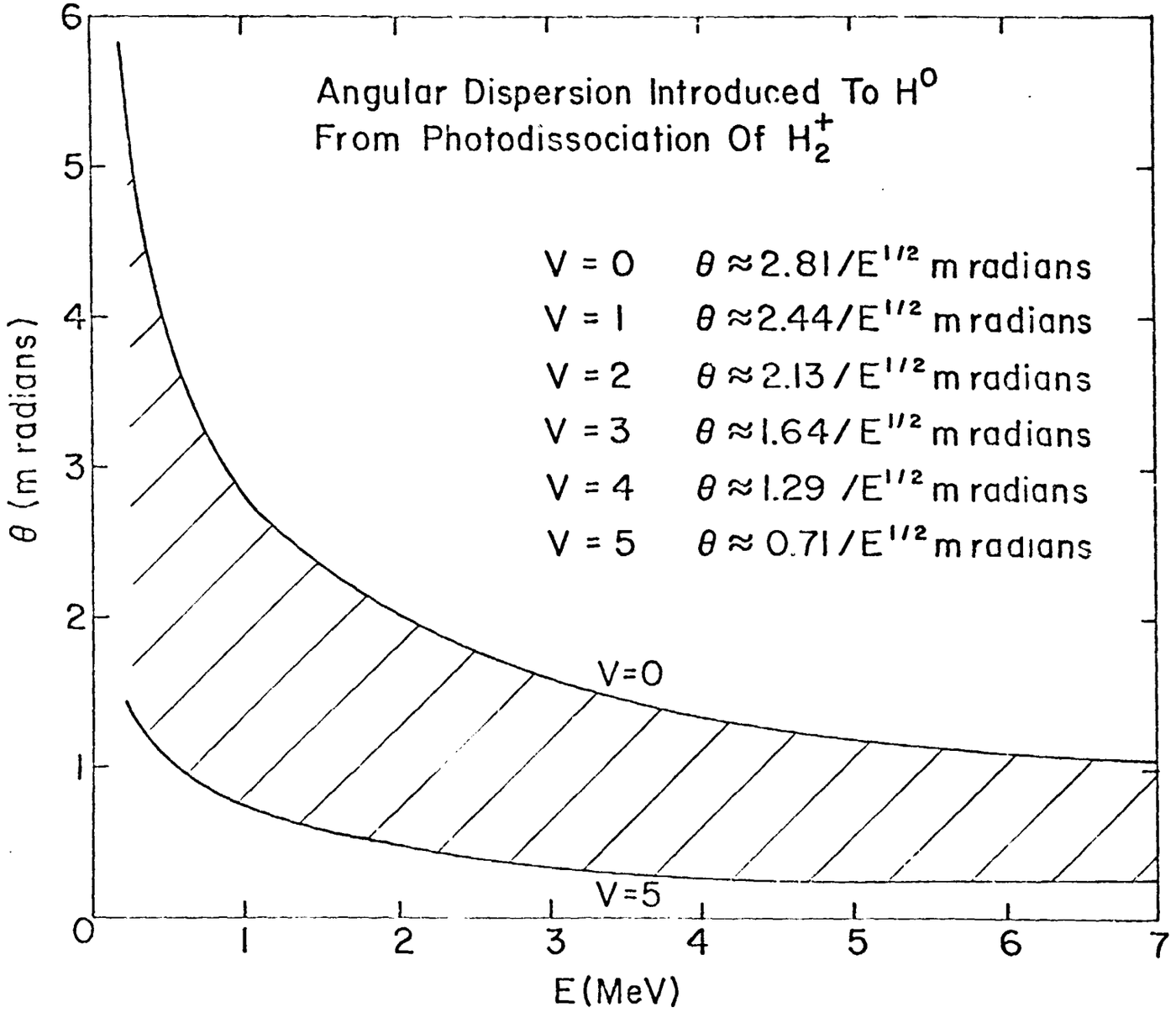

Fig. 5. Angular dispersion from the photodissociation of H_2^+.

MEASUREMENTS OF TRANSVERSE PHASE SPACE

The use of the laser diagnostic is to make detailed beam emittance measurements in an rf linac to evaluate sources of this growth. These detailed measurements can be used to calibrate computer codes to extrapolate to other conditions. The design of a high current linac depends on an ability to explore parametric variations reliably previous to the final construction of a full device.

The measurement of the phase space for an accelerator beam requires determination of the six variables x,x', y,y', $z,\dot{z}$, simultaneously (here f' denotes $df/dz = \dot{f}/\dot{z}$ where $\dot{f}$ denotes df/dt). Normally the quantities measured are projections coordinate axes or pairs of variables (x,x'), (y,y'), $(z,\dot{z})$ or (W,ϕ).

The initial measurements using the laser are simply to measure these projections for the transverse directions x and y. For the y direction, the laser beam axis lies along the x direction. The laser beam produces a neutral beam at $y = y_o$ with a width of about 0.1 mm. Because of the transverse velocity $\dot{y}$ the particle strikes a screen at a point $y_f = y_o + \dot{y}L/\dot{z}$, where L is the flight path length and $\dot{z}$ is the longitudinal speed of the particles at the neutralization point. Measurement of the position at which the particles strike the detector then allow determination of the y' values from the known y_o, $\dot{z}$, and L values. The procedures for the (x,x') phase space measurements are identical with the laser axis rotated by 90^o in the transverse plane.

Immediate questions are what range of y' values are expected and what distances are required to measure the phase space distributions accurately? The latter question is also related to limitations imposed by apertures of subsequent accelerator structures.

We assume the photodetachment process produces a neutral hydrogen atom that drifts from the production plane to the detection plane as illustrated in Fig. 6. The production zone may lie between drift tubes as shown or within the drift tube. For access to the drift tube interior, a hole the width of the beam long by 0.1 mm wide will need to be allowed in the drift tube wall.

The laser output is a single pulse of 25 to 30 ps time length. In space, the length of the pulse is 0.75 to 0.9 cm. The 25 ps pulse length for the laser is needed only to produce the neutral beam in a well defined region of space. Over the range of energies 0.25 to 7 MeV (β = 0.023 to 0.122) 25 ps represents motion of the H^- beam by only 0.17 to 0.92 mm in the longitudinal direction. This is the limiting spatial resolution that can be achieved in the longitudinal direction since the laser can be easily focused below 0. mm diameter for a distance (waist) of 7.4 mm.[6] For an acceptance phase of 40^o, the 25 ps time provides about 10 sampling positions within the beam micropulse (a 350 MHz frequency corresponds to 2.27 ns between micropulses).

The size of the production region is the waist size in the transverse plane. Figure 7 shows the production geometry. The distance from the geometrical centerline to the laser beam center (y) is known from the positioning of the laser beam. A reasonable error for a relative position measurement is 3 μm. The data is the distribution of particles (illustrated by h in Fig. 7) on the scintillation screen.

The initial problem is then to invert the particle distribution at $z_o + L$ to establish the transverse velocity distribution at z_o. The first observation we will make is that the distribution observed downstream from a line source is unique. Figure 8 illustrates this case by showing the physical

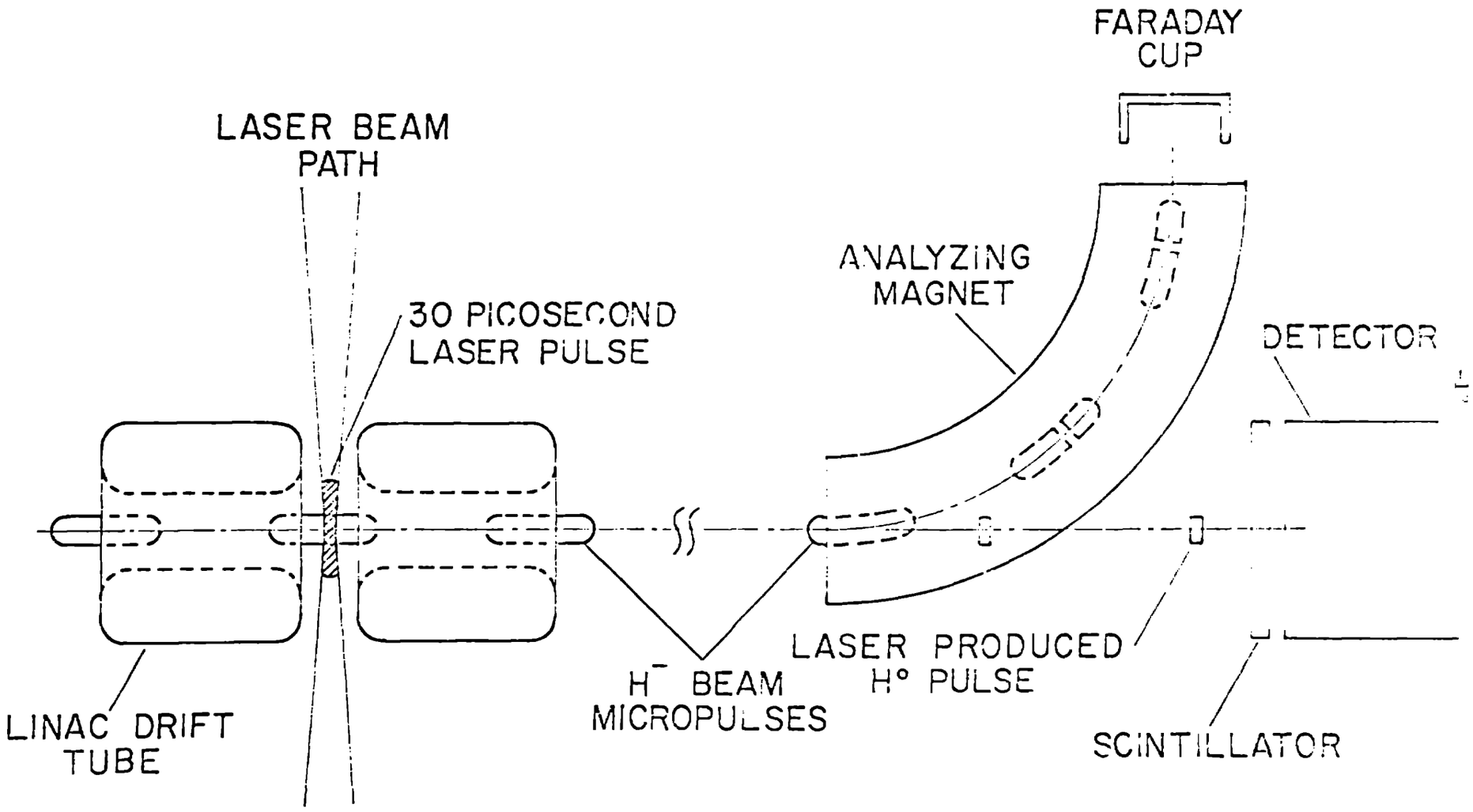

Fig. 6. Schematic diagram of experimental apparatus for measurement of phase space volume. The laser beam path is at z_o and the scintillator is at $z_o + L$.

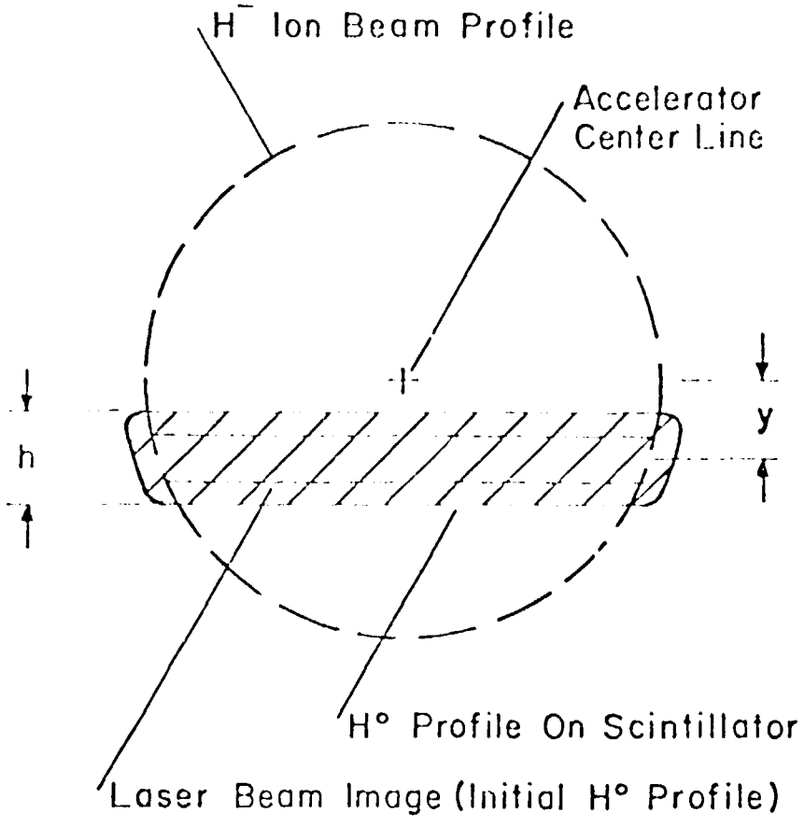

Fig. 7. Definitions of quantities used for transverse momentum measurement. The laser beam is located at $z = z_o$ and the distribution is measured at $z = z_o + L$

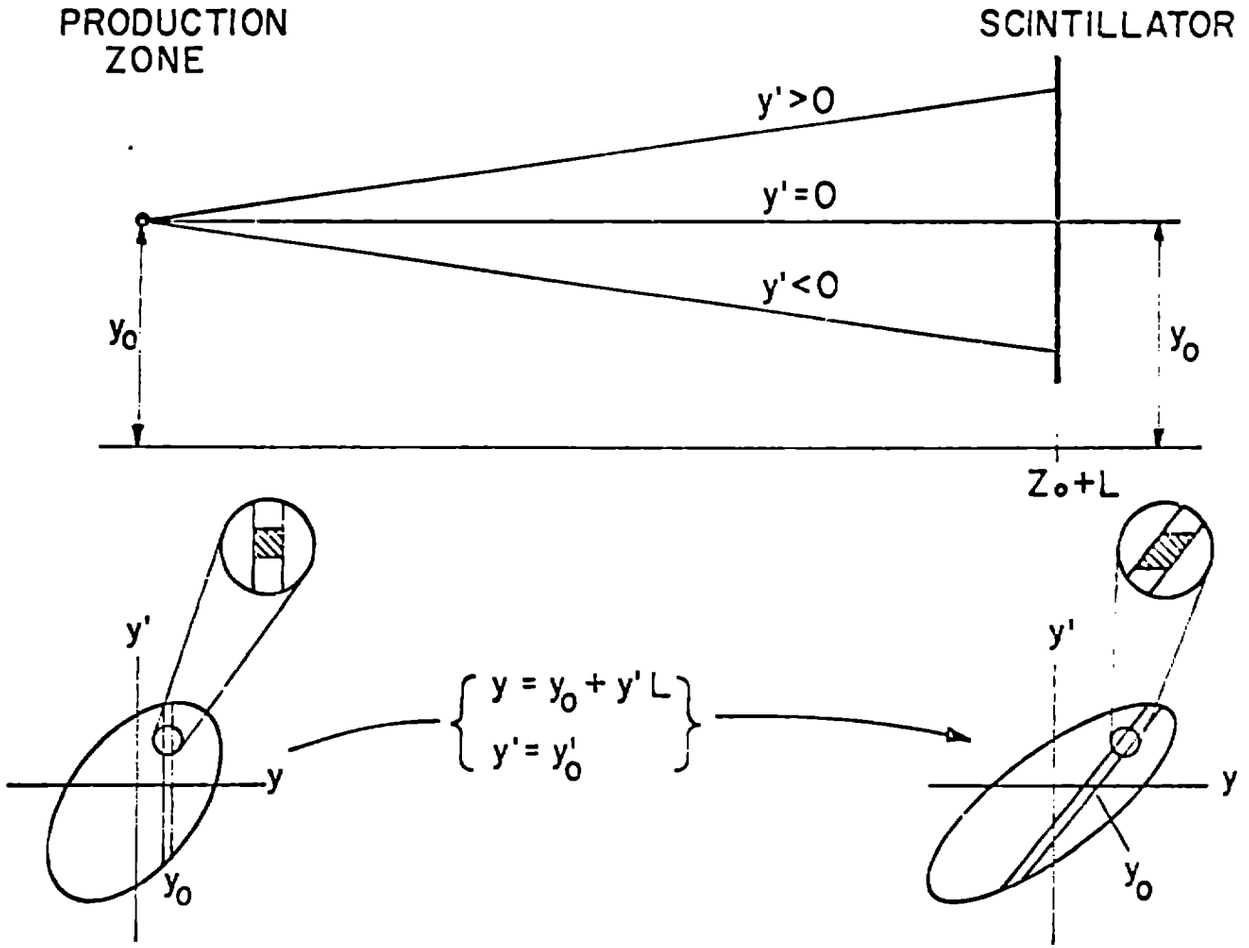

Fig. 8. Transverse phase space determination for a line photodetachment source function.

motions in the upper part of the figure and the phase space behavior in the lower part. The observed data distribution h at $z_o + L$ is related to the velocity distribution g at z_o by

$$g(y_o', z_o) = L\, h(y-y_o, z_o+L) \tag{7}$$

We remark that y_o and L are known from the accelerator alignment and the laser beam positioning devices. Because the drift transformation is a shear along the y axis of the phase space volume at constant density,[7] the resolution of the determination of the phase space at z_o is limited by finite beam size but the determination remains unique.

For the injector output, the divergence angle is expected to be about 380 μrad.[8] If the beam diameter is 3 mm, the beam edge profile will be y_{max} (mm) = 1.5 + 0.38 x 10^{-3} z(mm). For example, if the accelerator is 60 cm long, the diameter of the last drift tube bore should be 3.5 mm. If we assume sensitivity of 10 1/mm for the detector and a clear drift region of 2.5 m past the accelerator, the angular divergence measurable is 40 μrad or about 10% of the expected divergence. This implies that changes in phase space volume of about 10% are observable.

These calculations are applicable for a good quality beam. If we assume a 3 mm diameter beam and an 8 mm diameter bore tube the limits of the detectable phase space growth can be evaluated by assuming small beam diameter growth. The results of such a calculation are given in Fig. 9.

Since the manifestations of certain types of early phase space growth can be expected to occur later in the acceleration process[9,10] the problem of extracting the neutrals from the accelerator becomes even less important.

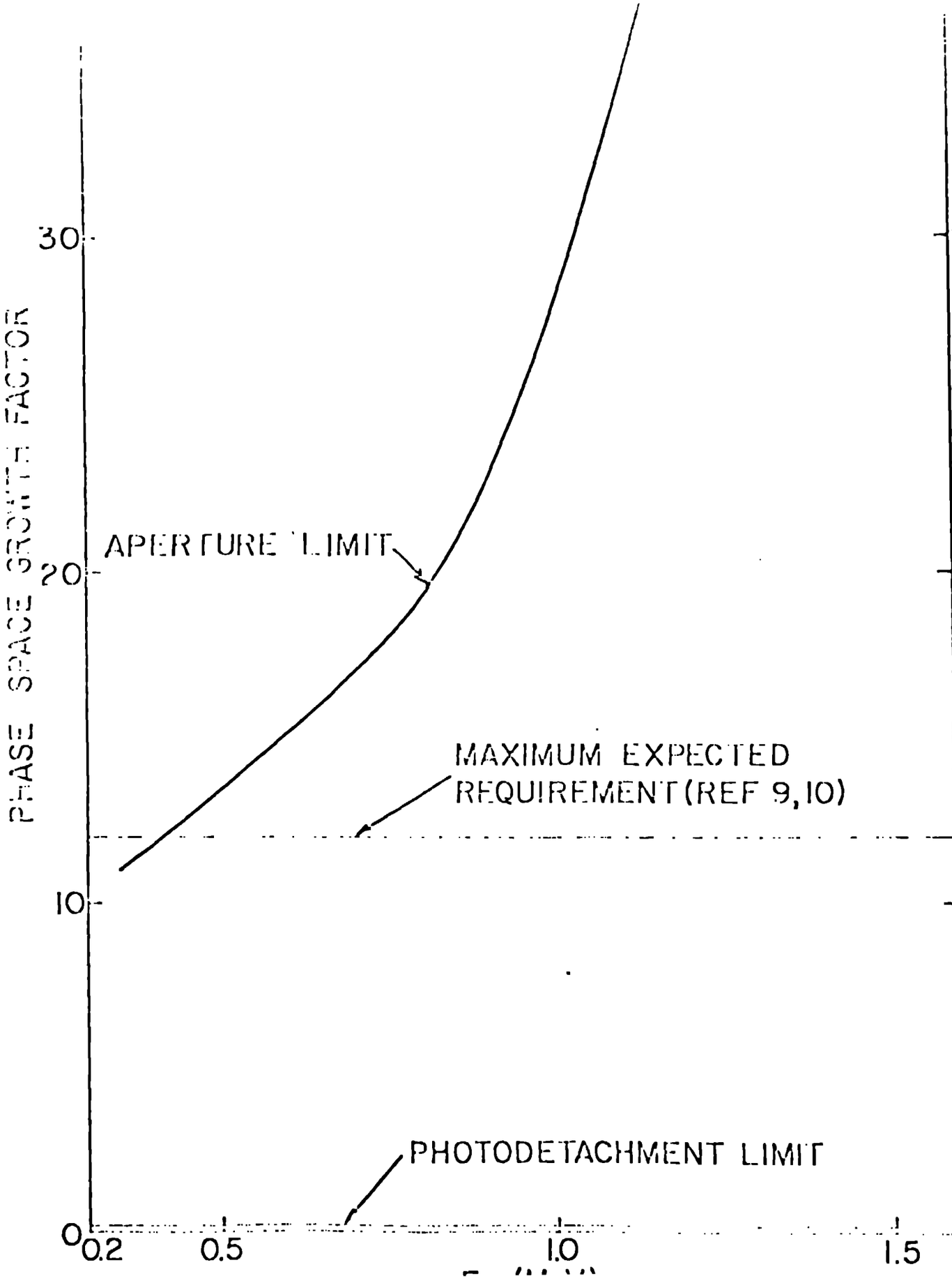

Fig. 9. Emittance growth observable for 3 mmp beam with 8 mmp
hore tubes assuming 0.35 mrad initial divergence and
2 MV/m accelerating electric fields (E_o = 4MV/m, ϕ_s=-60°)

LONGITUDINAL PHASE SPACE MEASUREMENTS

The determination of the phase space for the acceleration direction consists of measurement of the beam energy spread ΔW as a function of phase $\phi(=\omega t)$. Practically, therefore, the laser produces a neutral species at a known phase of the rf field and the energy spread of the neutral species is measured. The simplest method of detection is to use time-of-flight (TOF) on the neutrals. A more accurate method is a magnetic or electrostatic analyzer of charged particles (H^+) produced by stripping the neutrals following magnetic deflection of the H^- beam (cf Fig. 6). In this section we present results for limitations on the accuracy for each of these methods.

The TOF method obeys the equation

$$\Delta v/v = \Delta t/t \; ; \quad L = vt \quad . \tag{8}$$

Here L is the flight path length and Δt is the time resolution. Thus,

$$\Delta p/p = (\Delta t/L)\sqrt{\frac{2E}{m}} \tag{9}$$

For Δt = 2 ns and L = 10 m, this equation becomes

$$\Delta p/p = 2.77 \times 10^{-3} \sqrt{E(MeV)} \tag{10}$$

This is plotted in Fig. 10 as the lowest limit of the detection method. The time resolution of 2 ns surpasses currently available fast detector electronics, and 10 m is probably a maximum reasonable flight path length.

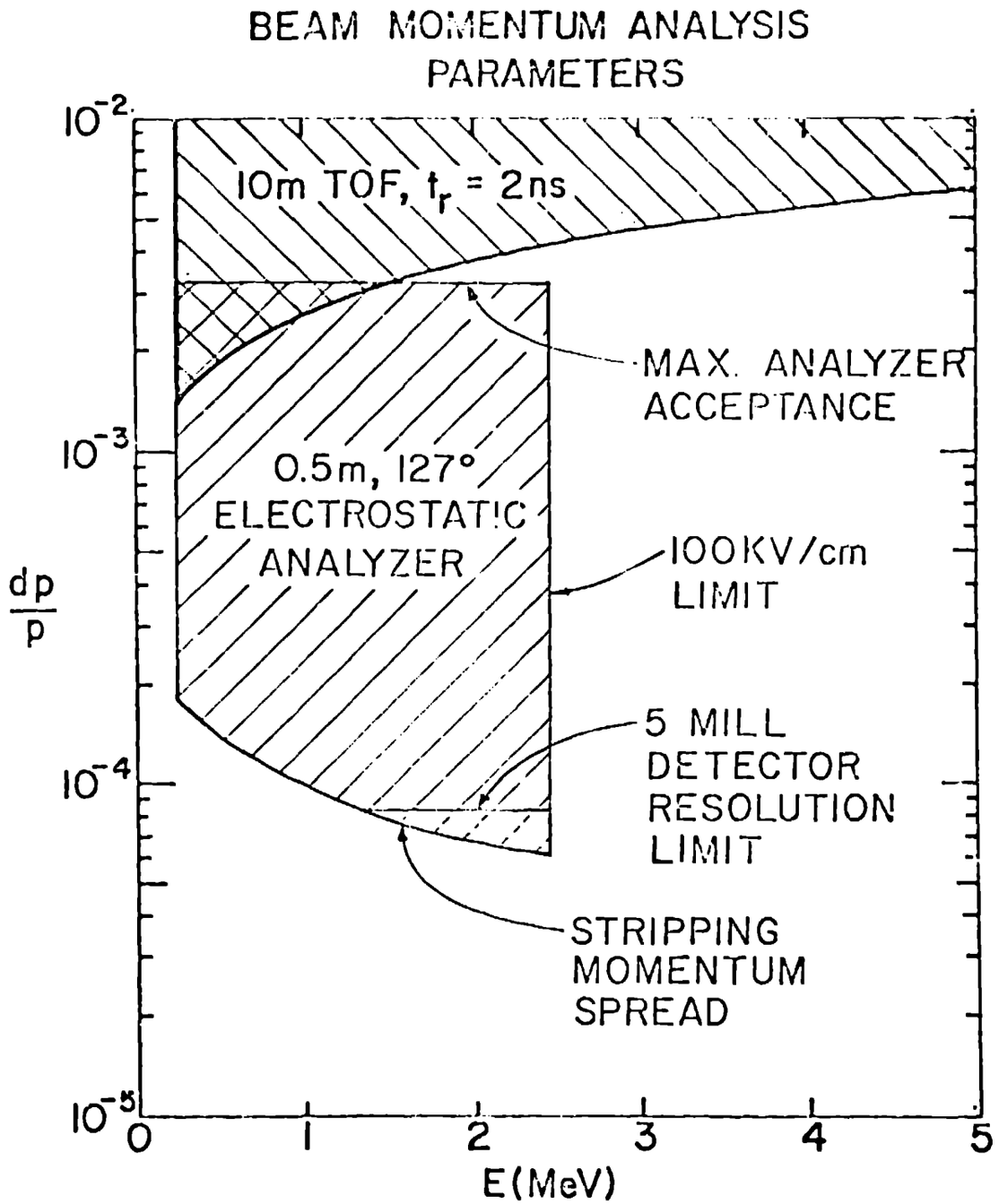

Fig. 10. Limitations for momentum spread measurements using various methods of measurements.

For higher resolution, a magnetic or electrostatic analyzer can be used. The best resolution obtainable with this method is limited by the stripping process. A previous experiment[11] has shown that the energy change of the system is only the binding energy of the hydrogen atom and the velocity change of the H^+ is only that needed to conserve energy and momentum. In the lab frame, the spread in energy is thus:

$$\Delta E \approx \pm 2 \sqrt{\frac{m_e}{m_p} E_o B} \tag{11}$$

where $m_e/m_p = 1/1836$ is the mass ratio for the electron and proton E_o is the hydrogen atom kinetic energy and B = 13.6 eV, the binding energy of the hydrogen atom.

$$\frac{\Delta p}{p} = \frac{1}{2} \Delta E/E_o = \sqrt{\frac{m_e B}{m_p E_o}} = 8.61 \times 10^{-5} / \sqrt{E_o(\text{MeV})} \tag{12}$$

For cylindrical analyzers, focus is obtained at 127° of flight path.[12,13] This means a divergent, monochromatic source obtains minimum size and thus highest resolution. For accuracy in energy determination, we suggest an electrostatic analyzer as the preferable device for this region of resolution. Reasonable size suggests about 0.5 m radius and maximum fields of 100 kV/cm leading to the indicated area in Fig. 10 where this method is applicable.

These methods should cover the region of interest for accelerators. We anticipate that TOF will meet many needs for analysis, particularly at lower energies, where effects of devices such as bunchers and acceleration voltage variations will be most influential on beam energy spread.

We note that if the capability for imaging at the detector is retained when the time dependence is measured, the data gives simultaneous longitudinal and transverse phase space information.

DETECTION OF THE NEUTRAL SPECIES

The rate of detection of the neutral particles is limited by the response of detectors. Scintillators[14,16] limit response to slower than about 10 ns due to their lifetimes of a few nanoseconds (see Table II). Solid state detectors are even slower. Direct production of charged particles at a metal surface can produce 1 to 2 ns pulses -- a limit imposed by multiplier time dispersion -- but spatial resolution is not retained for normal particle multipliers.

Thus, although sophisticated production configurations are possible, these detection limitations appear to limit their usefulness. An illustrative example of such a technique is given. Measurement of phase space behavior between successive micropulses could be of utility. The photoproduction of neutrals from successive micropulses is easily accomplished using a multipass cell set to place the light pulse from the laser at controlled points on successive micropulses by time-of-flight delay of the photons. An optical delay line cell composed of two spherical mirrors does this very effectively. Such cells have been used at LASL to reflect a He Ne laser up to 60 times and at Sandia Laboratories[17] to reflect dye laser light up to 100 times through the same focal spot. Since mirrors for 1.064 μm are available with greater than 99% reflectivity, 470 reflections are possible before reflection losses reduce the intensity to a level where the H^- photodetachment ceases to be complete (a 1.75 μJ per pulse leaves only 0.8% of the original H^- ions). Practically then the limit to the number of passes is the cell geometry, not mirror reflectivity.

TABLE 2

NE 102	Plastic	1.032	1.581	75	05	2.4	423		1.124	
NE 105	Plastic	1.037	1.58	75	05	2.4	423			
NE 110	Plastic	1.032	1.58	75	05	2.4	424		1.124	
NE 111	Plastic	1.032	1.581	75	05	2.4	425		1.124	
NE 113	Plastic	1.032	1.581	75	05	2.4	424		1.124	
NE 114	Plastic	1.032	1.581	75	05	2.4	424		1.124	
NE 140	Plastic	1.045	1.581	75	05	2.4	425	Sn 5%		
Pilot B	Plastic	1.032	1.581	75	05	2.18	425		1.124	
Pilot F	Plastic	1.032	1.581	75	05	2.4	425		1.124	
Pilot U	Plastic	1.032	1.581	75	05	1.66	424		1.124	
Pilot Y	Plastic	1.032	1.581	75	05	2.4	424		1.124	
NE 213	Liquid	0.874	1.508	141	60	3.7	425		1.213	
NE 216	Liquid	0.885	1.508	141	60	3.5	425		1.141	
NE 220	Liquid	1.035	1.492	104	60	3.8	425		1.080	
NE 221	Gel	1.03	1.492	104	60	4	425		1.080	
NE 224	Liquid	0.877	1.508	141	60	3.5	425		1.221	
NE 225	Liquid	1.01	1.508	141	60	3.5	425		1.221	
NE 228	Liquid	0.795	1.403	141	60	3.5	425		1.221	
NE 230	Deuterated liquid	0.945	1.469	141	60	3.5	425	D 14.2%	1.224	
NE 231	Liquid	1.08	1.50	141	60	4.28	425		1.224	
NE 232	Deuterated liquid	0.90	1.48	141	60	4.28	425	D 24.5%	1.195	
NE 233	Liquid	0.874	1.508	141	60	3.7	425		1.213	
NE 235A (235H)	Liquid	0.868	1.47	360	420 (50)	4.4	420		2.0	
NE 250	Liquid	1.035	1.492	104	60	4	425		1.080	
NE 260	Liquid				420		425			
NE 311 (311A)	B (^{10}B) loaded	0.91	1.411	85	60	3.8	425	B 5%	1.121	
NE 313	Gd loaded	0.98	1.505	136	60	4.0	425	Gd 0.5%	1.212	
NE 316	Sn loaded	0.93	1.486	148.5	60	4.0	425	Sn 10%	1.411	
NE 323	Gd loaded	0.979	1.50	101	60	3.8	425	Gd 0.5%	1.377	
NE 422 & 425	^{6}Li-ZnS(Ag)	2.36		110	300	200	450	Li 5%		
NE 451	ZnS(Ag)-plastic	1.443		110	300	200	450			
NE 901, 902, 903	Glass	2.64	1.58	~1000	28	75	395	Li 2.3%		
NE 904, 905, 906	Glass	2.5	1.55	~1000	55	18 & 60	395	Li 6.6%		
NE 907, 908	Glass	2.42	1.566	~1000	55	75	395	Li 7.5%		
NE 912, 913	Glass	2.3	1.55	~1000	28	75	395	Li 7.7%		
Anthracene	Crystal	1.25	1.62	217	100	30	447		0.715	
Stilbene	Crystal	1.16	1.626	125	150	4.5	410		0.956	
NaI(Tl)	Crystal	3.67	1.775	650	230	230	415			
NaI(pure)	Crystal	3.67	1.775	651	410*	60*	303*			
LiI(Eu)	Crystal	4.06	1.955	446	75	1200	475			
CsI(Tl)	Crystal	4.51	1.798	620	85	1100	565			
CsI(Na)	Crystal	4.51	1.787	621	150-190	650	420			
CsI(pure)	Crystal	4.51	1.788	621	15*	650*	420*			
CaF_2(Eu)	Crystal	3.17	1.443	1410	110	1200	385			
$CaWO_4$	Crystal	6.1	1.92	1535	35	6000	480			
ZnS(Ag)	Multi-crystal	4.09	2.356	1750	200	200	450			
ZnO(Ga)	Multi-crystal	5.61	2.02	1975	60	0.4	385			

*id nitrogen temperature.

14 for large area, high volume application.

The measurement of phase space for the same H^- pulse can reveal time or phase dependent phenomena. Such pulses can be generated using an echelle or thin film interference (Lummer-Gerke plate) to generate pulses spatially[13] (and thus temporally) separate. When these are shown on the beam, the pulses remove H^- ions in a machine gun fashion illustrated in Fig. 11. Observation of the pulses from these spatially separate beams does not require time resolution. By arranging the path differences for the light beams suitably, this method can be used to examine several points in different H^- beam micropulses as well.

A method for converting spatial information to time involves the use of fiber optics to provide the time delay. Since the index of refraction of the fibers is about 1.5, there is about 4.5 ns delay per meter of cable. Thus light observed by each fiber can be delayed to form a time dependent signal on a high gain device such as a photomultiplier tube by reasonable lengths of cable. One might also use the fiber as the scintillator and make a fiber optic harp.

ELECTRIC FIELD DETERMINATIONS

The TOF apparatus allows determination of electric fields in the gaps. For our accelerator the gap to cell length is approximately 5. The electric fields in the gap can be expected to range from approximately 15 to 40 MV/m. For a 0.1 mm beam, the beam spread will correspondingly be 1.5 to 4 keV due to electric field variations across the laser beam spot. At 250 kV near the low energy end of the accelerator $\Delta E/E \sim 1/250$ or $\Delta E \sim 1$ keV. (The electrostatic analyzer has much better resolution, of course.) Thus the electric field can be mapped with a resolution comparable to or better than about 2% by varying the laser position in the gap and observing the time-of-flight. The ion beam energy or ion beam spread gives local variation while the TOF variation gives the value of the electric field when the laser was fired.

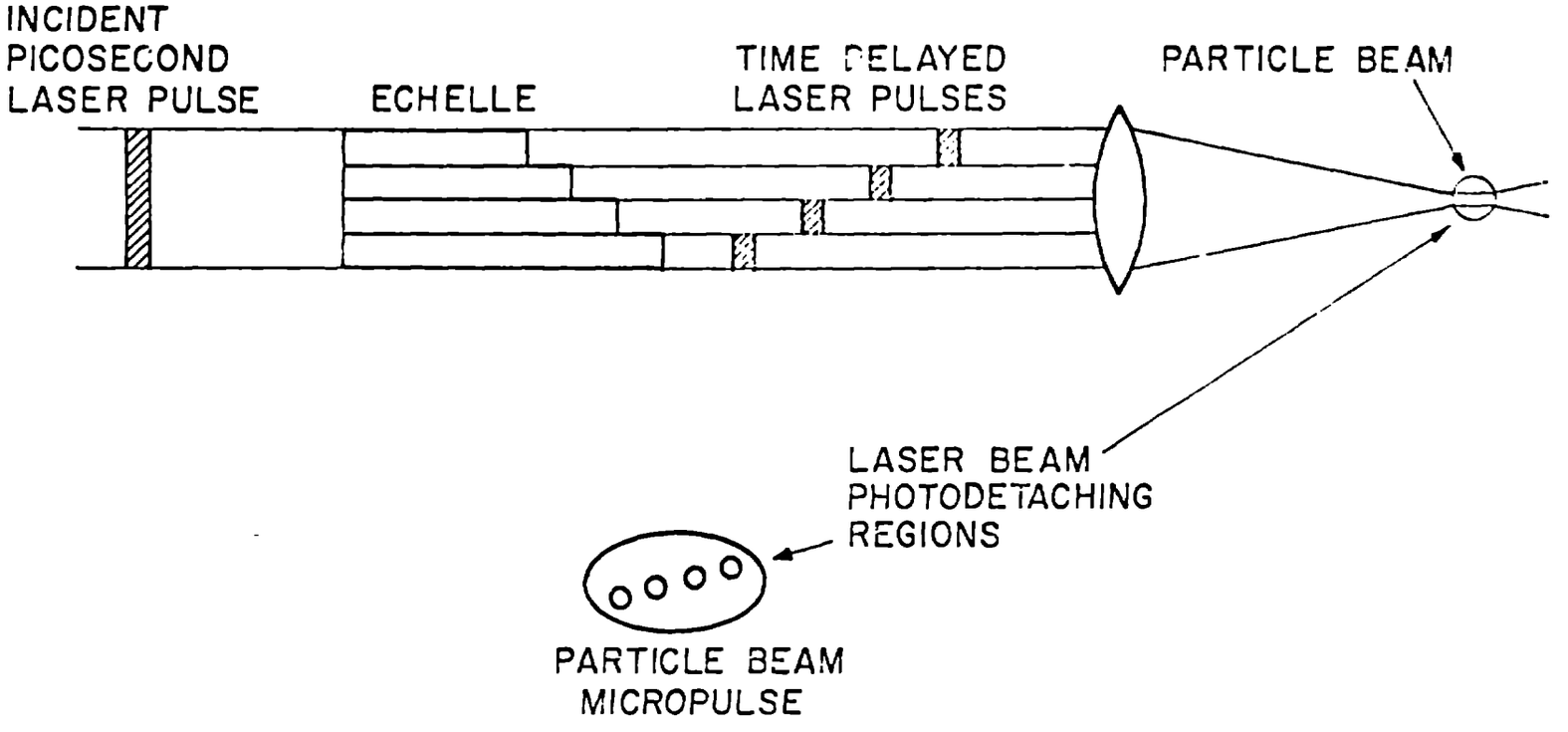

Fig. 11. Illumination of separate parts of a single beam micropulse by multiple laser pulses.

Since the variation of the electric field should decrease as space charge increases due to nonpenetration of the accelerating field into the ion beam, some information about fields within the ion beam plasma should be available from the measurements of ion energy spread as a function of beam current.

Since nonlinear optical processes are efficient (10 to 30%) methods of wavelength conversions at the high peak powers available from the picosecond lasers, frequency doubled (550 nm), tripled (354 nm), or quadrupled (266 nm) light at high intensity is available. The photon energy at 266 nm is 4.64 eV, higher than the work function of copper (4 to 4.5 eV). Thus electrons may be locally produced ($\sim$ 25 μm diameter spots) on the electrodes and used to measure electric fields by examining the x-ray end point energy produced by their impact with the opposite drift tube.

CONCLUSION

We have presented considerations for a laser based diagnostics for accelerator parameter measurement. Our expectations are

1. The physics of the diagnostic are sufficiently simple that more sophisticated methods of analysis than are currently used are not needed to understand the results.
2. Because the particles are neutral following photodetachment, space charge and electromagnetic field effects cease at the measuring point and results are not distorted by post production phenomena. These would occur for use of conventional diagnostics with high currents.[18,19]

REFERENCES

1. C. L. Perkins, Phys. Rev. 112, 1649 (1958).

2. L. M. Branscomb, Atomic and Molecular Processes, Ch. 4, Ed. by D. R. Bates, (Academic Press, NY, 1962).

3. H. S. W. Massey, E. H. S. Burhop, and H. B. Gilbody, Electronic and Ionic Impact Phenomena, Vol. II, p. 942 (Oxford at the Clarendon Press, London, 1969).

4. A. H. Kung, J. F. Young, and S. F. Harris, Appl. Phys. Lett. 22, 301, (1973) and Appl. Phys. Lett. 28, 239 (1975). See also M. H. R. Hutchinson, C. C. Ling, and D. J. Bradley, IQEC, Amsterdam, June 1978, referenced by D. H. Auston, Ultrashort Light Pulses, p 133, ed. by S. L. Shapiro, (Springer Verlag Berlin, 1977).

5. Gerhard Herzberg, Molecular Spectra and Molecular Structures I. Spectra of Diatomic Molecules, p. 538 (Van Nostrand Reinhold Co., NY, 1950).

6. A. E. Siegman, An Introduction to Lasers and Masers, pp 314-375 (McGraw Hill, NY, 1971).

7. John Farrell (private communication, 1979).

8. T. D. Hayward, FY-78 Annual Progress Report for Contract MIPR No. W31RPD-83-Z714 (1978) p. 56.

9. George E. Gillespie and Keith A. Brueckner, "Emittance Growth Studies Using a Travelling Wave Accelerator Model", Report PD-25-78-190, Contract DAAG 60-75-C-0080, January 5, 1978.

10. R. A. Jameson, LASL Memo AT-DO-377 (U), January 15, 1979 (to be published).

11. E. G. Bilpuch, F. O. Purser, J. D. Moses, T. D. Hayward, H. W. Newson, G. E. Mitchell, D. A. Outlaw and R. O. Nelson, "Note on High Resolution Measurements with a Tandem Accelerator", Nuclear Instruments and Methods, 113 (1973) pp 603-604.

12. Hermann Wollnik, Focussing of Charged Particles, Vol. II, Ch. 4.1, Ed. by Albert Septier (Academic Press, NY 1967).

13. Harold A. Enge, Focussing of Charged Particles, Vol. II, Ch. 4.2, Ed. by Albert Septier (Academic Press, NY, 1967).

14. V. O. Vyazemskii, I. I. Lomonosov, A. N. Pisarevskiy, Kh. V. Protopopov, V. A. Ruzin, and E. D. Teterin, Scintillation Method in Radiometry, pp 39-63 (State Publishing House for Atomic Energy and Technical Literature, Moscow, 1961).

15. S. C. Curran Luminescence and the Scintillation Counter, pp 67-95, 146 (Butterworth's Scientific Publications, London 1953).

16. Nuclear Enterprises Catalog.

17. A. Owyung, Sandia Labs, private communication. See also K. A. Hill and D. C. Hartley, Appl. Opt. 13 186 (1974).

18. E. P. Ippen and C. V. Shank, Ultrashort Light Pulses p 104, ed. by S. L. Shapiro (Springer-Verlag, Berlin, 1977).

19. M. Bacal and G. W. Hamilton, Phys. Rev. Lett. 42,2538 (1979).

20. L. R. Evans and D. J. Warner, "A Critical Study of Emittance Measurements of Intense Low Energy Proton Beams", CERN Report CERN/MPA/LIN 72-1 (1972).